Improved Along-Track Deformation Retrieval with ROSE-L using Two-Look ScanSAR

Simon Trumpf, Pau Prats-Iraola, Douglas Kotsubo, Dominik Richter, and Alberto Moreira
German Aerospace Center (DLR), Microwaves and Radar Institute, 82234 Wessling, Germany

Abstract

While deformation measurements in the line-of-sight direction using interferometric synthetic aperture radar (SAR) are state of the art, in most current spaceborne SAR systems they do not provide enough information to allow for inversion of all three spatial dimensions. Therefore, measurements in the along-track direction are crucial to enable 3-D displacement inversion with a SAR system like the upcoming ROSE-L mission. Recent study results have shown that the retrieval of along-track deformations with ROSE-L is possible using the two-look ScanSAR method, exploiting the angular diversity of the two looks, and hence achieving an accuracy better than the one provided by the azimuth resolution. The retrieval performance is hereby limited by system-inherent influences on the signal. This contribution presents three approaches to improve the performance and to partially mitigate resulting errors by using an adapted processing on ground, hence without changing the system itself. It is shown that the adapted processing can improve the overall retrieval performance.

1 Introduction

Deformation measurements with synthetic aperture radar (SAR) deliver important data for detecting, tracking and understanding various geophysical phenomena, such as earthquakes, landslides, glacier movement and volcanism [1]. SAR deformation measurements using the interferometric phase are one-dimensional, representing the deformation along the line of sight, thus multiple independent measurements are needed to separate the spatial components and to enable the retrieval of 3-D deformation fields. In most current spaceborne SAR systems the combination of coherent and incoherent interferometric measurement techniques can be used to separate deformation components along the track of the satellite and orthogonal to the track (referred to as zero-Doppler), however with a highly decreased accuracy of the along-track component with respect to the zero-Doppler component, for the along-track component is limited by the azimuth spatial resolution.

The future Radar Observing System for Europe in L-Band (ROSE-L) mission [2] has the potential to retrieve the along-track deformation component with an improved accuracy of about a factor 6 in the standard deviation with respect to correlation methods by using a two-look ScanSAR technique, which has been demonstrated in [3, 4] for the TerraSAR-X/TanDEM-X satellites and in [5] for the ALOS-2 satellite, among others. ROSE-L is a mission in the frame of the Copernicus Sentinel Expansion Missions led by the European Commission and supported by the European Space Agency. It consists of a constellation of L-Band radar sensors, using a ScanSAR acquisition mode and an antenna with five azimuth channels. The received signals of all five channels are downlinked and recombined on ground to reconstruct a wide bandwidth azimuth signal, allowing for the exploitation of burst overlaps for along-track deformation retrieval. The retrieval performance is hereby limited by the antenna pattern, which is optimized for single-look acquisitions rather than the exploitation of two looks. A modification of the transmit antenna pattern to improve the retrieval performance has been suggested in [6] and more recently in [7]; however, this comes at the expense of signal quality in the single-look bandwidth. In contrast, this contribution assumes an unchanged antenna pattern with respect to the current system design and presents a brief performance analysis of a two-look ScanSAR deformation retrieval together with three approaches to improve the retrieval accuracy during signal processing on ground.

The retrieval accuracy is driven by the signal-to-noise ratio (SNR) and the azimuth-ambiguity-to-signal ratio (AASR) of the reconstructed data. This is why the first approach uses a modified recombination of the subapertures' signals in order to increase the SNR of the measurement and the second approach increases the SNR by exploiting a third look. The third approach applies coherent azimuth ambiguity suppression techniques to improve the retrieval performance. The performance analysis of this contribution is focused on end-to-end simulations, the structure of which has been published in [8]. The presented contribution furthermore extends the analytic results from [9] and is structured as follows. First, in Section 2 the along-track deformation retrieval algorithm is briefly summarized, including the relevant performance metrics. Section 3 then presents the adapted processing for increased performance, specifically the cascaded beamforming (Section 3.1), the exploitation of a third look (Section 3.2) and the coherent azimuth ambiguity removal (Section 3.3). Section 4 shows an exemplary full simulation and, finally, Section 5 draws the conclusions of the presented results.

2 Along-track deformation retrieval

The along-track deformation retrieval is based on the exploitation of ScanSAR burst overlaps, which, due to their different azimuth Doppler centroids, show different sensitivities to the along-track component of the deformation. By computing the difference of the interferometric phases of both looks for a specific target, the along-track component of the deformation can be inverted from the measured deformations in line of sight. The performance of this retrieval technique is limited by the accuracy of the interferometric phase, which is driven by the SNR and the AASR, as analyzed in detail in [8]. The resulting effects are demonstrated using a simulation of a two-look acquisition over eastern Turkey, using the reflectivity of a Sentinel-1 acquisition together with a artificial deformation field, modeled with the Okada model [10], and a temporal decorrelation assumed constant with $\gamma_{\text{temp}} = 0.7$ as inputs to the simulation [8]. Three bursts of the simulation of a single sub-swath are shown in **Figure 1**.

SNR and AASR are both significantly influenced by the system's antenna pattern. As in the case of ROSE-L the antenna pattern is not optimized for an exploitation of two looks, a decrease in coherence towards the burst edges can be observed from the simulated coherence in Figure 1a. This decrease in coherence leads to increased noise in the interferometric phase, as shown in Figure 1b. In addition to the increased phase noise, also phase biases caused by coherent azimuth ambiguities can be observed. When computing the differential interferometric phase, these measurement errors appear in the signal as well, as is shown in Figure 1c. The unwrapped differential interferometric phase $\phi_{\text{dinf, uw}}$ can then be converted to the along-track deformation $d_{\text{along-track}}$ by multiplying with a conversion factor depending on the sensor velocity over ground v_g and the spectral separation of the two looks in the azimuth Doppler spectrum Δf. The conversion is then given by [3, 5]

$$d_{\text{along-track}} = \phi_{\text{dinf, uw}} \cdot \frac{v_g}{2\pi\Delta f}. \tag{1}$$

Figure 1d shows the deformation measurement derived from the differential interferometric phase for the present simulation.

The two error components –noise and biases– can be separated in the simulation, as shown in Figure 1e. While the noise can be partially mitigated by spatial averaging, the biases are more complex to remove. Further simulation results have shown that the measurement biases due to coherent azimuth ambiguities can be even stronger than in the given example, to a degree where a proper unwrapping of the differential interferometric phase would not be possible [8]. This case occurs for scenarios with a very heterogeneous backscatter and large differences in the local interferometric phases, e.g. glaciers. In these cases, ambiguity removal algorithms can help with the mitigation of potential measurement errors.

3 Performance optimization

To improve the measurement accuracy, noise and ambiguity biases have to be reduced. The phase noise can be reduced by spatial averaging, leading to a more coarse resolution [8]. Another approach to improve the SNR, preserving the original resolution, is based on the multi-channel structure of the ROSE-L system. As a larger bandwidth than required for the two-look mode is reconstructed, an additional beamforming step could be used to increase the SNR [9]. The second optimization approach proposes the partial exploitation of a third look to increase the SNR.

Furthermore, an algorithm to suppress coherent azimuth ambiguities is proposed. Several algorithms for compensating coherent azimuth ambiguities on interferogram level exist, which could be also applied to the along-track deformation retrieval case. The one presented in this contribution is based on the algorithm proposed in [14].

3.1 Cascaded beamforming

The ROSE-L antenna consists of five subapertures, used as independent receive channels for the radar signal. Those five channels are downlinked and recombined into a single receive signal during the on-ground processing. Commonly, an algorithm based on a least-squares estimation is used for this step, as for example proposed in [11]. This algorithm reduces aliasing within the subsampled channel signals, reconstructing a total bandwidth of $B_{\text{rec}} = N_{\text{ch}} \cdot \text{PRF}$, where N_{ch} is the number of channels used for the reconstruction (ROSE-L: $N_{\text{ch}} = 5$) and PRF the pulse repetition frequency. As B_{rec} is larger than the bandwidth required for the two-look processing, it is possible to reduce the number of channels used for the reconstruction, using M subsets of $N < N_{\text{ch}}$ channels, and add a separate step of maximum-steering beamforming with the M reconstructed signals to improve the SNR. This is referred to [N + M]-beamforming in this paper and is similar to an approach proposed in [12]. The reconstruction can be expressed as an inversion, where a signal $u_{[N]}$ is reconstructed from N aliased signals u_n in N spectral intervals f_n, with $n = 1, \ldots, N$, given as

$$\begin{bmatrix} u_{[N]}(f_1) \\ \vdots \\ u_{[N]}(f_N) \end{bmatrix} = \begin{bmatrix} P_1(f_1) & \cdots & P_N(f_1) \\ \vdots & \ddots & \vdots \\ P_1(f_N) & \cdots & P_N(f_N) \end{bmatrix} \cdot \begin{bmatrix} u_1 \\ \vdots \\ u_N \end{bmatrix}, \tag{2}$$

where $P_q(f_p)$ is the reconstruction factor of the qth channel signal on the pth frequency interval. In the next step, the M reconstructed channels are weighted and summed as

$$u_{[N,M]} = \sum_{m=1}^{M} w_m u_{[N]m}, \tag{3}$$

where $u_{[N,M]}$ is the signal after a N-channel reconstruction and M-channel beamforming, $u_{[N]m}$ is the mth reconstructed signal and w_m is the beamforming weight. The latter is computed as [12]

$$w_m = \frac{1}{M} \cdot \exp\left\{ j\pi \cdot \frac{\Delta x_m}{v_{\text{s}}} \cdot f_{\text{az}} \right\}, \tag{4}$$

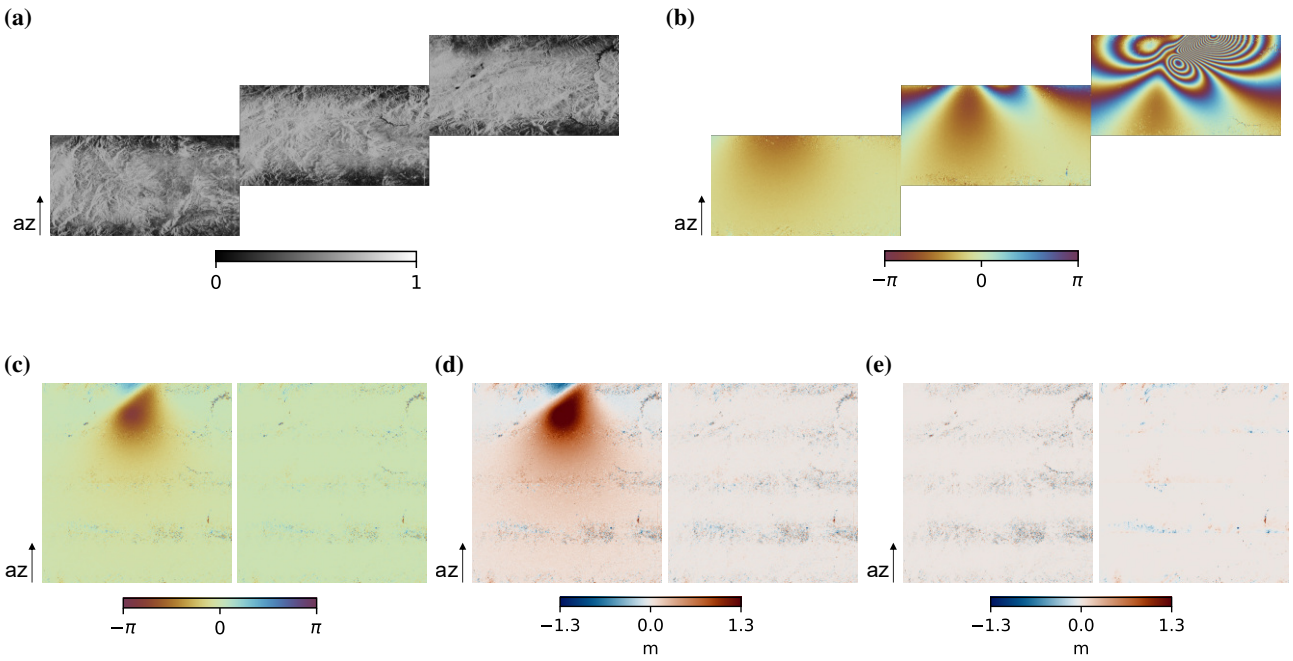

Figure 1 Deformation retrieval with the two-look ScanSAR simulation showing three consecutive bursts. (a) Coherence and (b) Interferometric phase. (c) Differential interferometric phase and error. (d) Along-track deformation measurement and error. (e) Noise and ambiguity error contributions.

where f_{az} is the frequency in the azimuth Doppler spectrum, v_s the satellite velocity and Δx_m the distance between phase center of the reconstructed channels and phase center of the complete antenna array. Note that this beamforming step is also performed in the range-Doppler domain.

The effect on the noise can then be quantified as a noise scaling factor Φ_{casc}, a function of the ratio between the SNR of the cascaded beamforming ($\mathrm{SNR}_{\mathrm{casc}}$) with respect to the SNR of a single channel signal ($\mathrm{SNR}_{\mathrm{ch}}$), compared to the reference case, where all channels are used for the reconstruction ($\mathrm{SNR}_{\mathrm{full}}$), with the PRF where uniform sampling is achieved ($\mathrm{PRF}_{\mathrm{uni}}$). The scaling factor follows as

$$\Phi_{\mathrm{casc}} = \left(\frac{\mathrm{SNR}_{\mathrm{casc}}/\mathrm{SNR}_{\mathrm{ch}}}{(\mathrm{SNR}_{\mathrm{full}}/\mathrm{SNR}_{\mathrm{ch}})|_{\mathrm{PRF}_{\mathrm{uni}}}} \right)^{-1} = \frac{1}{N} \left| \mathbf{A}_M \right|^2, \tag{5}$$

where $\mathbf{A}_M$ is a scaling matrix, computed from the cascaded reconstruction matrix $\mathbf{P}_{\mathrm{casc}}$ and the beamforming weights, given as

$$\mathbf{A}_M = \mathbf{P}_{\mathrm{casc}} \mathbf{w}_{\mathrm{bf}} = \begin{bmatrix} P_1 & 0 & \cdots & 0 \\ \vdots & P_1 & \ddots & \vdots \\ P_N & \vdots & P_1 & 0 \\ 0 & P_N & \vdots & P_1 \\ \vdots & \ddots & P_N & \vdots \\ 0 & \cdots & 0 & P_N \end{bmatrix} \cdot \begin{bmatrix} w_1 \\ \vdots \\ w_M \end{bmatrix}. \tag{6}$$

The exact increase in SNR with respect to the full reconstruction hereby depends on the PRF. For the first subswath of ROSE-L, an increased SNR by up to 1dB was reached, while keeping azimuth ambiguities at a reasonable level. In this case, the cascade beamforming was performed with $N = 4$ and $M = 2$ (i.e. [4 + 2]-beamforming). The interested reader is referred to [9] for a more detailed theoretical analysis. Note that the referenced paper assumes fully decorrelated ambiguities, while the simulation in the present paper works with coherent ambiguities, where the temporal coherence of signal and ambiguities are assumed the same.

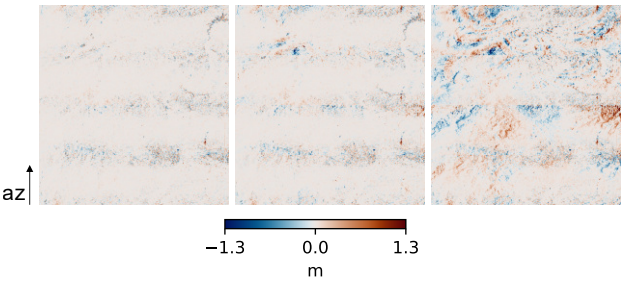

Figure 2 Cascaded beamforming results on the simulated scene. Left: Full reconstruction; Center: [4 + 2]; Right: [3 + 3]

The results in **Figure 2** show the measurement error with the same simulated scene as in Figure 1. While the improved SNR is only barely visible, the increased azimuth ambiguity biases due to the decreased number of channels in the reconstruction can be clearly identified.

To evaluate the impact of the increased SNR on the measurement accuracy, the deformation measurement of a second simulation is evaluated. For this purpose, we generate a homogeneous scene of distributed scatterers with

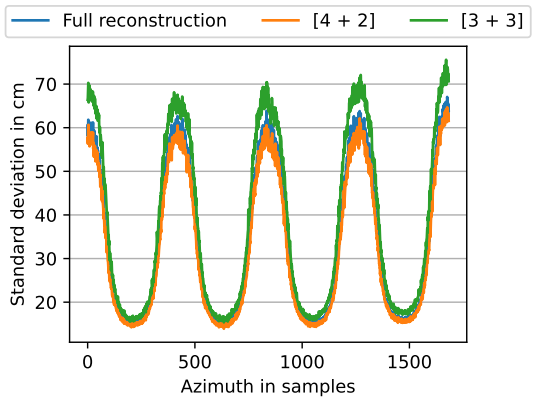

Figure 3 Standard deviation over the range dimension of the along-track deformation measurement error with a homogeneous scene.

backscatter $\sigma_0 = -25\,\mathrm{dB}$. By computing the standard deviation of the measurement error over range, we compare the measurement accuracy as a function of the azimuth position. **Figure 3** shows the standard deviation of all range samples plotted over the azimuth sample position, showing a slightly decreased standard deviation for the [4 + 2]-reconstruction with respect to the full reconstruction reference. Also here, the large ambiguity increase in the [3 + 3]-reconstruction case leads to a lower measurement accuracy than the reference. The small measurement performance increase is in line with the results from [9].

3.2 Exploitation of a third look

A second approach to increase the SNR of the measurement includes the further exploitation of the available bandwidth by using a third look. In case the full bandwidth is available for processing, an even larger overlap could be processed allowing for the processing of an additional look. As the spectral separation of the outer looks and the one closest to zero-Doppler is the same, two differential interferograms could be computed and averaged in order to reduce phase noise while maintaining the same resolution. Simulation results have shown that this approach indeed increases the SNR in certain areas close to the two-look burst edges. **Figure 4** shows the simulated scene, processed with an additional third overlapping burst for 50% of all pixels. Due to the significantly decreasing SNR towards the edges of the extended bursts, an exploitation of the third look for the remaining 50% of the pixels would lead to a decreased measurement accuracy in these areas. Furthermore, the exploitation of a third look will introduce more biases due to coherent azimuth ambiguities. The effect of the increased SNR is again analyzed stochastically with the same homogeneous scene as in Figure 3. The resulting standard deviation of the error is shown in **Figure 5**.

3.3 Coherent ambiguity removal

Given the small orbital tube of the ROSE-L repeat-pass interferometric acquisition mode and the resulting small interferometric baselines, ambiguities correlate and contribute a coherent signal which biases the signal of interest. These biases cannot be mitigated by averaging or additional beamforming. Instead, an algorithm to estimate and coherently subtract the biases from the interferograms is proposed based on [14]. A block scheme of the proposed removal algorithm is shown in **Figure 6**.

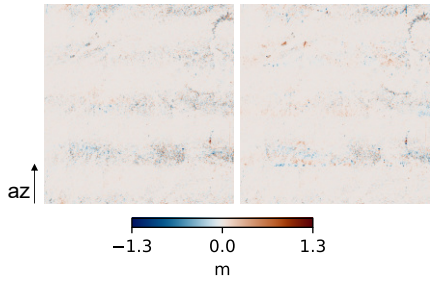

Figure 4 Extended overlap processing results on the simulated scene. Left: Two looks; Right: Partial three looks (50%).

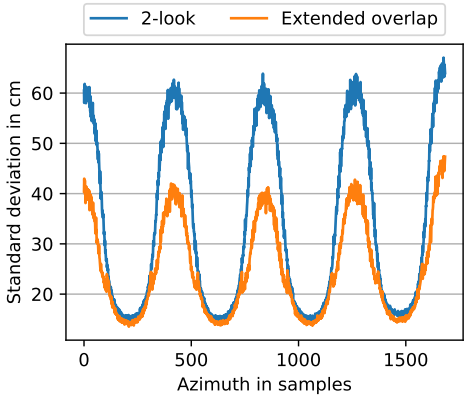

Figure 5 Standard deviation over the range dimension of the along-track deformation measurement error with a homogeneous scene.

As derived in [13], the ambiguous signal can be modeled as a complex sum of main signal and coherent ambiguities. Hence, a first estimate of the ambiguous component of the interferogram can be obtained by combining estimates of ambiguity amplitude, coherence and interferometric phase. In a next step this estimate can be used to subtract the ambiguous signal. The computation of the in-

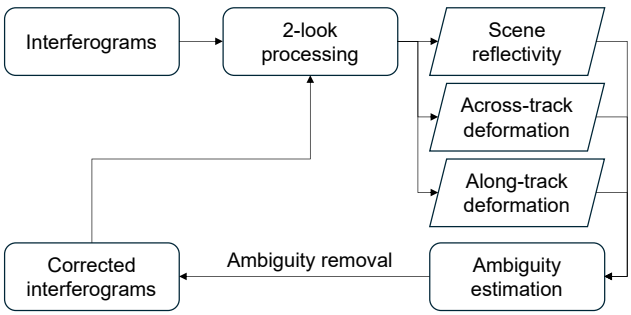

Figure 6 High-level block diagram of the ambiguity removal algorithm.

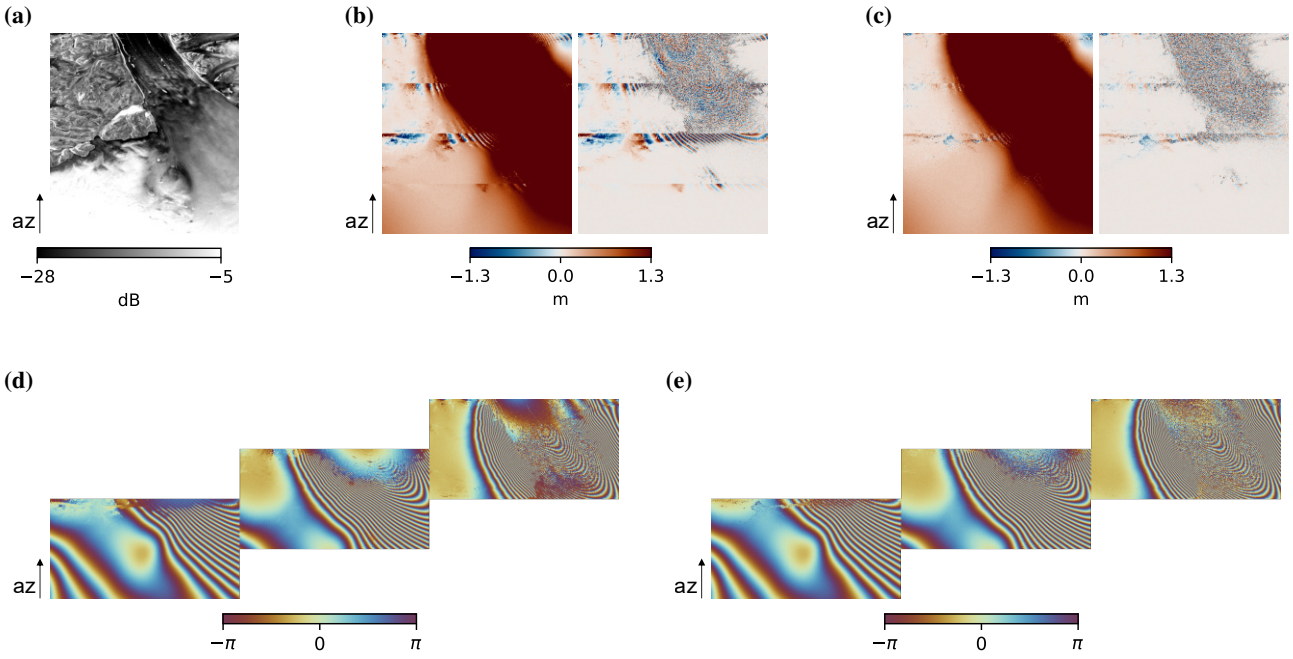

Figure 7 Along-track deformation retrieval with the glacier scene, before and after ambiguity removal. (a) Amplitude of the focused SAR image. (b) Initial along-track deformation measurement and error. (c) Corrected along-track deformation measurement and error. (d) Interferometric phase without ambiguity removal. (e) Interferometric phase with ambiguity removal.

terferometric phase is however not trivial, as it requires an unbiased retrieval result. We propose to iteratively retrieve deformation and correct for systematic errors to retrieve an unbiased deformation map. Furthermore, this approach relies on the assumption that the mean backscatter of a target does not vary as a function of the Doppler centroid.

To demonstrate the ambiguity removal, results from a different simulation with stronger ambiguity biases are shown in **Figure 7**. The scene is located around a highly decorrelated glacier tongue, where the combination of high backscatter in the ambiguity origin area, together with lower backscatter around the glacier and the increasing AASR towards the burst edges cause significant measurement biases. With the given removal algorithm, these biases are partially suppressed in the interferograms, which can then be used to compute a new along-track deformation estimate. The corrected interferograms still show some residual biases. As the algorithm itself is unbiased, these residual biases are likely caused by ambiguity model mismatches, such as sub-pixel shifts and mismatches in the impulse response, which are currently being investigated. As an alternative, an adapted version of the algorithm proposed in [15] may also be applied. The algorithm has shown to relax the necessary assumptions and requirements with respect to the precise knowledge of the before mentioned error sources, which may be further improving the suppression performance.

4 Exemplary results

To show the deformation retrieval results over a larger area, the full simulation results of both previously introduced scenes are shown in **Figure 8**. Both simulations take the reflectivity of a Sentinel-1 subswath (approx. $300\,\mathrm{km}$ in azimuth and $80\,\mathrm{km}$ in ground range) together with a given deformation as input. The interested reader is referred to [8] for more details about the structure of the simulations. Due to the different error contributions within the given scenes, the simulation over Turkey is exploiting a third look to increase the SNR where needed as shown in Section 3.2, while the simulation over the glacier compensates azimuth ambiguities as presented in Section 3.3.

5 Conclusions

The presented results show that the along-track deformation measurements accuracy with ROSE-L can be increased by applying the three proposed techniques. Which technique –or which combination of techniques– is most effective, depends on the scene. Scenes with low noise impact and strong ambiguities will not benefit from cascaded beamforming, while for scenes with strong noise impact and small biases, improving the SNR might be sufficient. In general, all three techniques could also be applied in conjunction, note, however, that the presented techniques to increase the SNR will in return increase the ambiguity bias and vice versa, so the tradeoff between ambiguities and noise cannot be avoided by applying multiple techniques at the same time.

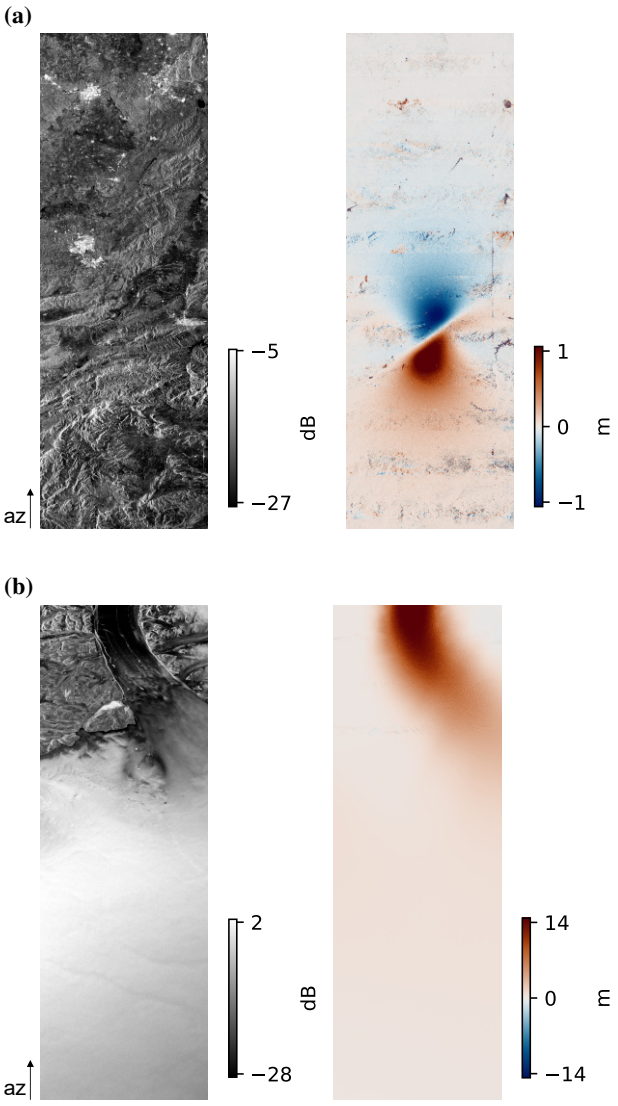

Figure 8 Full simulated scenes. Left: Amplitude of the de-bursted image. Right: Measured along-track deformation. (a) Scene over eastern Turkey with deformation simulated based on the Okada model. (b) Scene over the Petermann glacier in Greenland, with realistic deformation input.

Furthermore, the application of the two-look technique in general –and even more the proposed exploitation of a third look– require the availability of at least the two-look bandwidth after the reconstruction. This would require the storage of twice the amount of data, hence having a clear impact in the ground segment of the mission. On the other hand, a clear advantage of the proposed technique is that no changes are needed within the satellite system itself, hence preserving the image quality of the single-look products.
The exploitation of the proposed approach would allow the retrieval of accurate 3-D deformation measurements, as well as the computation of the interferometric phase in zero-Doppler direction, which is beneficial for phase unwrapping as it removes phase jumps at the burst edges. Further applications would also benefit from the larger angular diversity, e.g., ionospheric mitigation.

6 Literature

[1] J. Biggs and T. J. Wright, “How satellite InSAR has grown from opportunistic science to routine monitoring over the last decade,” Nat. Commun., vol. 11, no. 1, pp. 1–4, Aug. 2020.

[2] D. Geudtner et al., “Copernicus ROSE-L SAR mission,” in Proc. 14th Eur. Conf. Synth. Aperture Radar (EUSAR), pp. 1–4, Jul. 2022.

[3] N. Yague-Martinez et al., “Experimental validation with TerraSAR-X/TanDEM-X of advanced interferometric modes for accurate retrieval of azimuthal displacements,” Proc. IEEE Int. Geosci. Remote Sens. Symp. (IGARSS), pp. 1444–1447, Jul. 2016.

[4] N. Yague-Martinez, P. Prats-Iraola, S. Wollstadt, and A. Moreira, “The 2-look TOPS mode: design and demonstration with TerraSAR-X,” IEEE Trans. Geosci. Remote Sens., vol. 57, no. 10, pp. 7682–7703, Oct. 2019.

[5] C. Liang and E. J. Fielding, “Measuring azimuth deformation with L-band ALOS-2 ScanSAR interferometry,” IEEE Trans. Geosci. Remote Sens., vol. 55, no. 5, pp. 2725–2738, May 2017.

[6] S. Perna et al., “A conceptual performance study on a two-look ScanSAR mode configuration for the forthcoming ROSE-L mission,” IEEE Trans. Geosci. Remote Sens., vol. 62, pp. 1–18, 2024.

[7] S. Perna et al., "Two-look ScanSAR mode configuration with ROSE-L: Toward an effective and easily implementable solution," ESA Living Planet Symposium, Jun. 2025.

[8] S. Trumpf, P. Prats-Iraola, and A. Moreira, “Along-track deformation retrieval performance with the ROSE-L multichannel SAR system using two-look ScanSAR,” IEEE Trans. Geosci. Remote Sens., vol. 63, pp. 1–15, 2025.

[9] S. Trumpf, P. Prats-Iraola, and A. Moreira, “Cascaded digital beamforming on receive with the ROSE-L multichannel SAR system for along-track deformation retrieval,” IEEE Geosci. Remote Sens. Lett., vol. 23, pp. 1–5, 2026.

[10] Y. Okada, “Surface deformation due to shear and tensile faults in a half-space,” Bull. Seismol. Soc. Amer., vol. 75, no. 4, pp. 1135–1154, Aug. 1985.

[11] G. Krieger, N. Gebert, and A. Moreira, “Unambiguous SAR signal reconstruction from nonuniform displaced phase center sampling,” IEEE Geosci. Remote Sens. Lett., vol. 1, no. 4, pp. 260–264, Oct. 2004.

[12] N. Gebert, G. Krieger, and A. Moreira, “Digital beamforming on receive: Techniques and optimization strategies for high-resolution wide-swath SAR imaging,” IEEE Trans. Aerosp. Electron. Syst., vol. 45, no. 2, pp. 564–592, Apr. 2009.

[13] M. Villano and G. Krieger, “Impact of azimuth ambiguities on interferometric performance,” IEEE Geosci. Remote Sens. Lett., vol. 9, no. 5, pp. 896–900, Sep. 2012.

[14] P. Lopez-Dekker, Y. Li, L. Iannini, P. Prats-Iraola, and M. Rodriguez-Cassola, “On azimuth ambiguities suppression for short-baseline along-track interferometry: the Stereoid case,” in Proc. IEEE Int. Geosci. Remote Sens. Symp. (IGARSS), IEEE, Jul. 2019.

[15] D. Richter, M. Rodriguez-Cassola, M. Zonno, and P. Prats-Iraola, "Coherent Azimuth Ambiguity Suppression Based on Linear Optimum Filtering of Short Along-Track Baseline SAR Interferograms," in Proc. 14th Eur. Conf. Synth. Aperture Radar (EUSAR), pp. 1-5, Jul. 2022.